Dyes and Pigments 91 (2011) 26–32

Contents lists available at ScienceDirect

Dyes and Pigments

journal homepage: www.elsevier.com/locate/dyepig

Functionalized magnetic core–shell Fe_3O_4@SiO_2 nanoparticles as selectivity-enhanced chemosensor for Hg(II)

Xiaohong Peng, Yujiao Wang, Xiaoliang Tang, Weisheng Liu*

Key Laboratory of Nonferrous Metals Chemistry and Resources Utilization of Gansu Province and State Key Laboratory of Applied Organic Chemistry, College of Chemistry and Chemical Engineering, Lanzhou University, Lanzhou 730000, PR China

ARTICLE INFO

Article history:
Received 4 November 2010
Received in revised form
27 January 2011
Accepted 31 January 2011
Available online 23 March 2011

Keywords:
Chemosensor
Turn-on
Colorimetric
Hg^{2+}
Fe_3O_4@SiO_2 nanoparticles
Magnetic separation

ABSTRACT

A colorimetric and "turn-on" fluorescent chemosensor Rho-Fe_3O_4@SiO_2 for Hg^{2+} in which N-(rhodamine-6G)lactam-ethylenediamine (Rho-en) is conjugated with the magnetic core–shell Fe_3O_4@SiO_2 NPs has been strategically designed and synthesized. The final product was characterized by X-ray power diffraction (XRD), transmission electron microscopy (TEM), Fourier transform infrared spectra (FTIR) and UV–visible absorption and fluorescence emission. Fluorescence and UV–visible spectra results showed that the resultant multifunctional nanoparticles Rho-Fe_3O_4@SiO_2 exhibited selective 'turn-on' type fluorescent enhancements and distinct color changes with Hg^{2+}. The selectivity of the Rho-Fe_3O_4@SiO_2 for Hg(II) ion is better than that of the Rho-en in the same conditions. In addition, the presence of magnetic Fe_3O_4 nanoparticles in the sensor Rho-Fe_3O_4@SiO_2 NPs would also facilitate the magnetic separation of the Hg(II)–Rho-Fe_3O_4@SiO_2 from the solution.

1. Introduction

Detection of heavy transition metal (HTM) ions, such as Pb^{2+}, Cd^{2+}, Cu^{2+} and Hg^{2+} [1–4], has received considerable attention, owing to potential environmental and biological implications [5]. Especially, the detection of Hg^{2+} has attracted continuous attention, because it can causes serious environmental and health problems. Hg^{2+} can easily pass through skin, respiratory, and gastrointestinal tissues into the human body, where a very small amount of Hg^{2+} could damage the central nervous and endocrine systems [6]. Accordingly, the development of new or improved analytical methods for the sensitive and selective determination of Hg^{2+}, which are applicable in a wide range of different sites and environments, is highly desirable. To date, a number of selective small-molecular Hg^{2+} sensors have been devised. However, their use in related analytical techniques in the homogeneous phase is not suitable for the separation, removal and enrichment of target species or in rapid screening applications.

Magnetic core–shell Fe_3O_4@SiO_2 nanoparticles as special immobilizing carrier of biomolecules have aroused great interest in current researches because they are biocompatible, easily renewable, and are stable against degradation [7–12]. The inner iron-oxide core with outer shell of silica not only stabilizes the nanoparticles in solution but also provides sites for surface modification with various biomedical ligands in biomedical applications [13,14]. Usually, an inert silica coating on the surface of magnetite nanoparticles prevents their aggregation in solution, improves their chemical stability, and provides better protection against toxicity [15]. The silica coating stabilizes the magnetite nanoparticles in two different ways [16]. One is by shielding the magnetic dipole interaction with the silica shell. On the other hand, the silica nanoparticles are negatively charged. Therefore, the silica coating enhances the coulomb repulsion of the magnetic nanoparticles. However, magnetic nanoparticles have not been frequently used to separate and remove toxic environmental pollutants.

Rhodamine-based fluorescent chemosensors have received increasing interest because of their high fluorescence quantum yield, broad range of absorption and emission wavelengths (extended to the visible region), and large absorption coefficients [17]. Whereas rhodamine derivatives with spirolactam structure are nonfluorescent and colorless, the presence of a metal cation, such as Cr^{6+} [18], Cr^{3+} [19,20], Fe^{3+} [21–25], Cu^{2+} [26–30], Hg^{2+} [31–44], Pb^{2+} [45], Cd^{2+} [46], and Ag^{+} [47,48] can result in ring-opening of the spirolactam via coordination or irreversible chemical reaction, which accompanied by the appearance of a pink color and high fluorescence intensity. Recently, the modification of different Rhodamine-based fluorescent

* Corresponding author. Tel.: +86 931 8915151; fax: +86 931 8912582.
E-mail address: liuws@lzu.edu.cn (W. Liu).

0143-7208/$ – see front matter © 2011 Elsevier Ltd. All rights reserved.
doi:10.1016/j.dyepig.2011.01.012

chemosensors on the surface of nanostructured materials, including ultrathin platinum films [49], copolymer micelle [50], Mesoporous Silica [51] and nanoparticles [52] have been reported for detection of various metal ions.

In our work, an attempt has been made that the magnetic core–shell Fe_3O_4@SiO_2 nanoparticles are functionalized by Rhodamine-based fluorescent chemosensor. Herein, we report the synthesis of a colorimetric and "turn-on" fluorescent chemosensor Rho-Fe_3O_4@SiO_2 for Hg^{2+}, in which N-(rhodamine-6G)lactam-ethylenediamine (Rho-en) is conjugated with the magnetic core–shell Fe_3O_4@SiO_2 NPs. The magnetic property of Fe_3O_4 nanoparticles in the Rho-Fe_3O_4@SiO_2 NPs would facilitate the magnetic separation of the Hg(II)–Rho-Fe_3O_4@SiO_2 from the solution, while the silica nanoshell would stabilize the magnetic NPs and provide sites for surface modificated with organic chemosensor.

2. Experimental section

2.1. Materials

3-(Triethoxysilyl)propyl isocyanate, tetraethoxysilane (TEOS) were purchased from Alfa Aesar Chemical Company. $FeCl_2 \cdot 4H_2O$, $FeCl_3 \cdot 6H_2O$, ammonium hydroxide (14%) were purchased from Aihua Chemicals Ltd. Toluene was used after purification by standard methods. Other chemicals were used as received without further purification.

2.2. Preparation of magnetite Fe_3O_4 nanoparticles

The magnetite nanoparticles were synthesized based on a slight modification of a published one-pot chemical coprecipitation method [53]. First, the deionized water was purged with nitrogen gas for 20 min. Then, $FeCl_3 \cdot 6H_2O$ (9.60×10^{-3} kg), $FeCl_2 \cdot 4H_2O$ (4.00×10^{-3} kg), and oleic acid (1.70×10^{-3} dm^3) were added to deionized water (0.03 dm^3) under nitrogen atmosphere with vigorous stirring. The mixture solution was heated to 90 °C. Then, ammonium hydroxide (0.04 dm^3) (14 wt %) was added rapidly to the solution, and it immediately turned black. The reaction was kept at 90 °C for 5 h and then allowed to cool to room temperature. The black precipitate was collected by centrifugation at 10,016 g for 30 min and resuspended in chloroform with an end concentration of 5.45×10^{-2} kg oleic acid-capped Fe_3O_4/dm^3

2.3. Synthesis of Fe_3O_4@SiO_2 nanoparticles

The Fe_3O_4 coated SiO_2 nanoparticles were synthesized by a similar procedure developed by Lu et al. [54]. Two mg of oleic acid-capped Fe_3O_4 nanoparticles was suspended in cyclohexane (0.01 dm^3) at room temperature. Then Triton X-100 (1.8×10^{-3} kg), hexanol (1.6×10^{-2} dm^3), and H_2O (0.34×10^{-3} dm^3) were added with stirring to form water-in-oil microemulsion. After 15 min, TEOS (4×10^{-5} dm^3) was added to the mixture. One-half hour later, aqueous ammonia (28–30 wt %, 0.01 dm^3) was added to initiate the TEOS hydrolysis and condensation. After 24 h, ethanol was added to destabilize the microemulsion system and precipitate the Fe_3O_4@SiO_2 nanoparticles. The Fe_3O_4@SiO_2 nanoparticles were isolated via centrifugation and washed with ethanol five times and deionized water five times to remove adherent surfactant and unreacted chemicals.

2.4. Synthesis of Rho-Si and Rho-Fe_3O_4@SiO_2 nanoparticles (Scheme 1)

Rho-en (5×10^{-4} mol) was dissolved in dry toluene (0.03 dm^3). To the solution, 3-(triethoxysilyl) propyl isocyanate (5×10^{-4} mol) was added at room temperature. The reaction mixture was refluxed for 5 h at the nitrogen atmosphere. The solvent was evaporated and the product was isolated by column chromatography on silica gel

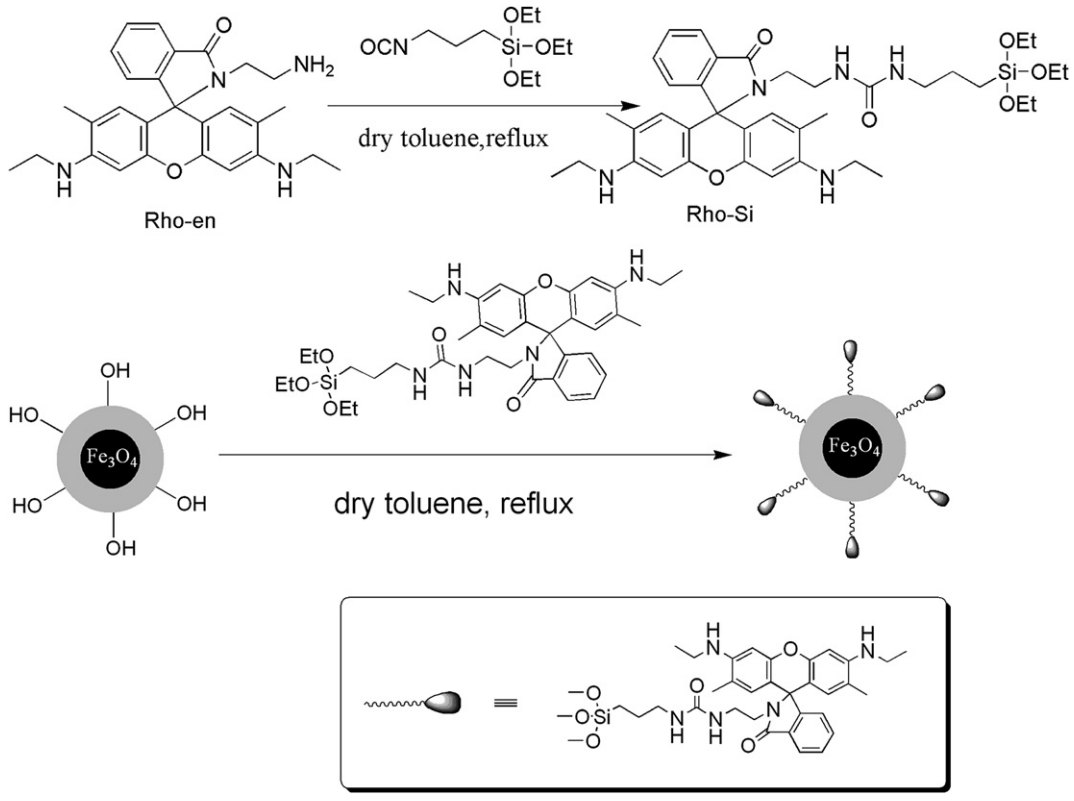

Scheme 1. Synthesis of Rho-Si and Rho-Fe_3O_4@SiO_2.

(ethyl acetate). Yield: 69%. ESI-MS: m/z 704.5 ($M + H^+$). ^1H NMR ($CDCl_3$, 400 MHz): 0.62 (t, 2H, CH_2Si); 1.10–1.34 (t, 15H, CH_3); 1.59 (m, 2H, CH_2); 1.96 (s, 6H, Ar-CH_3); 3.21–3.26 (m, 6H, $NHCH_2$); 3.82 (q, 6H, $SiOCH_2$); 2.89–3.14 (t, 4H, NCH_2CH_2NH); 6.22–7.89 (8H, Ar). ^{13}C NMR ($CDCl_3$, 400 MHz): 7.64 (CH_2Si); 14.67–18.27 (CH_3); 23.60–58.33 (CH_2); 65.56 (C); 96.55, 105.38, 118.11, 122.70, 123.87, 128.07, 128.10, 130.59, 132.69, 147.51, 151.68, 153.78 (Ar); 157.95 (NH–C=O); 169.47 (Ar–C=O).

And then the Fe_3O_4@SiO_2 nanoparticles 1×10^{-4} kg and 3.52×10^{-4} kg (0.5×10^{-3} mol) Rho-Si were suspended in 0.04 dm^3 of anhydrous toluene. The mixture was stirred for 24 h at 90 °C at the nitrogen atmosphere. The functionalized Fe_3O_4@SiO_2 nanoparticles were collected by centrifugation and repeatedly washed with anhydrous toluene, dichloromethane, and then ethanol under ultrasonic condition. Unreacted organic materials were removed completely by monitoring the fluorescence of the washed liquid.

2.5. Characterization and test of the materials

Dupont-1090 thermal gravimetric analysis (TGA) instrument, transmission electron microscopy (TEM, Hitachi-600, Japan) with an accelerating voltage of 100 kV were used to characterize the materials. IR spectra were recorded on Nicolet FT-170SX instrument using KBr discs in the 400–4000 cm^{-1} region. ^1H NMR and ^{13}C NMR spectra were measured on a Brucker DRX 400 spectrometer in CD_3OD solution with TMS as internal standard. Chemical shift multiplicities are reported as s = singlet, t = triplet, q = quartet and m = multiplet. Mass spectra were recorded on a Bruker Daltonics esquire6000 Mass spectrometer. UV absorption spectra were recorded on a Varian Cary 100 spectrophotometer using quartz cells of 1.0 cm path length. Fluorescence measurements were made on a Hitachi F-4500 spectrophotometer and a shimadzu RF-540 spectrofluorophotometer equipped with quartz cuvettes of 1 cm path length with a xenon lamp as the excitation source. An excitation and emission slit of 5.0 nm were used for the measurements in the solution state. All spectrophotometric titrations were performed with a suspension of the sample dispersed in CH_3CN.

3. Results and discussion

3.1. XRD

The structural properties of synthesized Rho-Fe_3O_4@SiO_2 were analyzed by X-ray power diffraction (XRD). As shown in Fig. 1, XRD patterns of the synthesized Fe_3O_4@SiO_2 and Rho-en coated Fe_3O_4@SiO_2 display several relatively strong reflection peaks in the 2θ region of 20–70°, which is quite similar to those of Fe_3O_4 nanoparticles reported by other group [55]. The discernible six diffraction peaks in Fig. 1 can be indexed to (2 2 0), (3 1 1), (4 0 0), (4 2 2), (5 1 1) and (4 4 0), which match well with the database of magnetite in JCPDS (JCPDS Card: 19-629) file. Besides the peak of iron oxide, the XRD pattern of iron-oxide/SiO_2 core–shell nanoparticles (Fig. 1) presented a broad featureless XRD peak at low diffraction angle, which corresponded to the amorphous state SiO_2 shells.

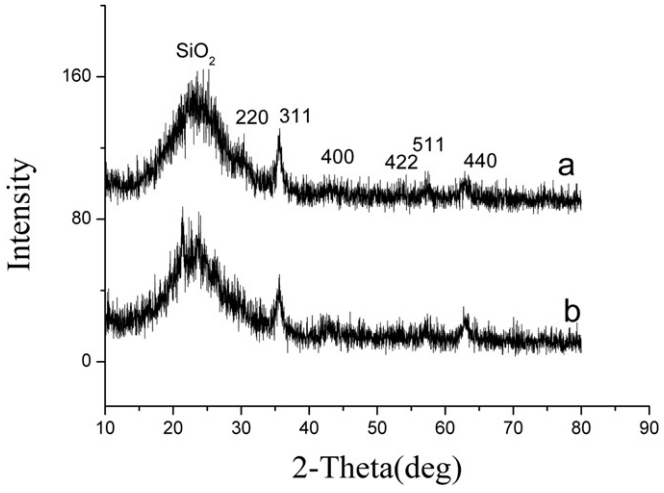

Fig. 1. XRD patterns of Fe_3O_4@SiO_2 (a) and Rho-Fe_3O_4@SiO_2 (b).

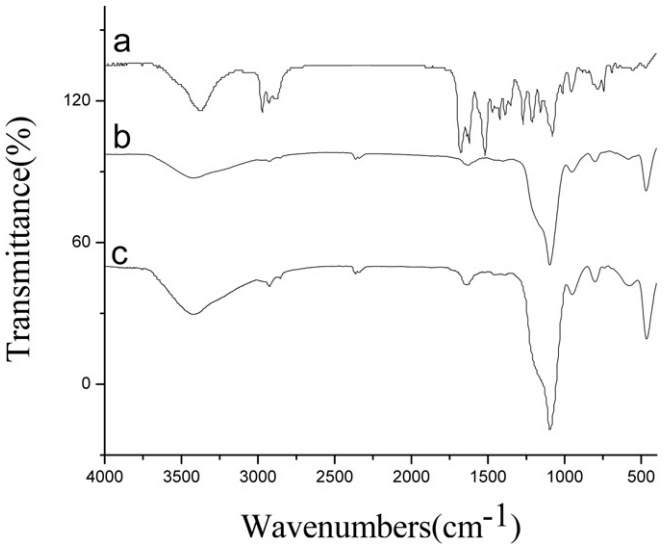

Fig. 2. IR spectra of Rho-Si (a), Fe_3O_4@SiO_2 (b) and Rho-Fe_3O_4@SiO_2 (c).

3.2. FTIR

The successful conjugation of Rho-en onto the surface of the Fe_3O_4@SiO_2 nanoparticles can be confirmed by infrared (IR). The bands at 3400–3500 cm^{-1} and 1000–1250 cm^{-1} of the both samples are ascribed to the O–H and Si–O stretching vibration on

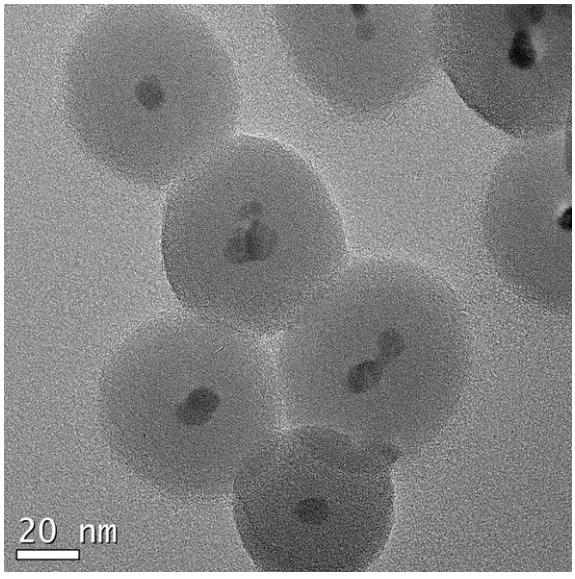

Fig. 3. TEM images of Rho-Fe_3O_4@SiO_2.

silanol. Rho-Fe_3O_4@SiO_2 exhibited a ν_{lactam}(C═O) vibration at 1638 cm^{-1}, red-shifted from 1684 cm^{-1} in Rho-en (Fig. 2). These shifts indicate that Rho-en couples to Fe_3O_4@SiO_2 nanoparticles through −NCO.

3.3. TEM

Transmission electron microscopy (TEM) revealed that iron-oxide nanoparticles had entrapped in the silica shell successfully, in which an average particle size is about 50–60 nm and the diameter of the magnetic core is about 10 nm (Fig. 3).

3.4. Magnetic property

The magnetic hysteresis loop of the magnetic nanoparticles Rho-Fe_3O_4@SiO_2 measured at $T = 300$ K (close to room temperature) is shown in Fig. 4a. It demonstrated that the magnetic silica sphere was in superparamagnetic regime at room temperature, as evidenced by zero coercivity and resonance of the magnetization loop. Our measurement was consistent with the conclusion that magnetic Fe_3O_4 nanoparticles smaller than 20 nm are usually superparamagnetic at room temperature [56]. The superparamagnetic property of the particle is very important for its biological application. It can prevent the magnetic nanoparticles from aggregating. On the other hand, it can enable the particles to redisperse rapidly when the magnetic field is removed. The saturation magnetization (*Ms*) value of Rho-Fe_3O_4@SiO_2 is measured to be 6.24×10^3 emu/kg. Complete magnetic separation of Rho-Fe_3O_4@SiO_2 was achieved in 1 min by placing a magnet near the vessels containing the CH_3CN dispersion of the nanoparticles (Fig. 4b). The magnetic separation capability of Fe_3O_4@SiO_2 nanoparticles in this detection method can also offer a simple route to separate Hg(II)–Rho-Fe_3O_4@SiO_2 system from various environment.

3.5. Fluorescence properties

On the basis of the results of EA, about 0.068 mol/kg of Rho-Si is loaded on the support. Changes in the fluorescence properties of Rho-Fe_3O_4@SiO_2 as a result of the addition of other metal ions,

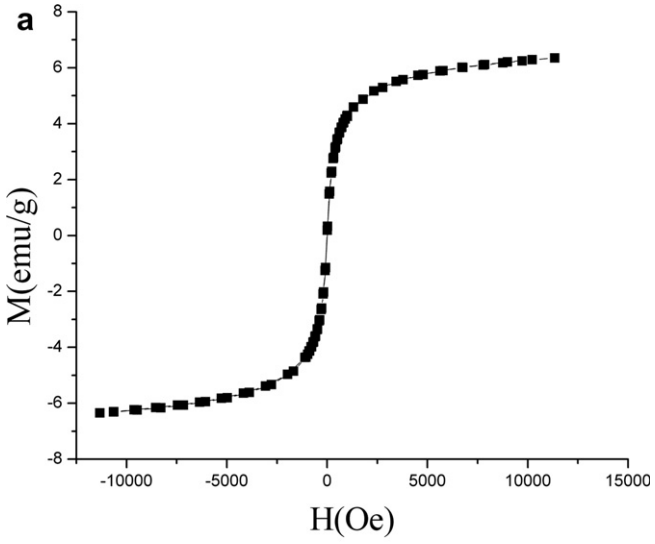

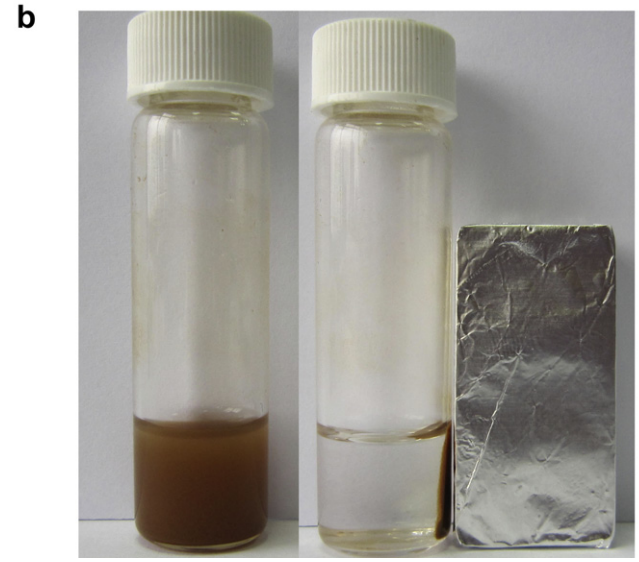

Fig. 4. (a) Magnetization curves of the Rho-Fe_3O_4@SiO_2; (b) (A) Rho-Fe_3O_4@SiO_2 was dispersed in CH_3CN; (B) Rho-Fe_3O_4@SiO_2 responded to an external magnet.

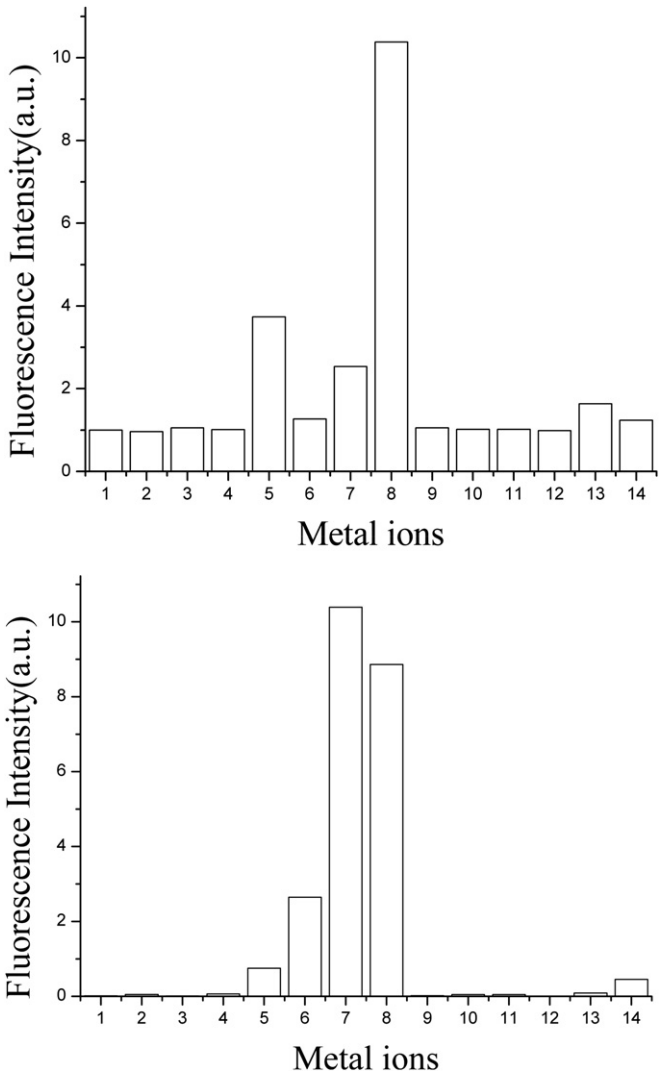

Fig. 5. Fluorescence response of Rho-Fe_3O_4@SiO_2 (a) (0.3 g/L) and Rho-en (b) (10 μM) to various cations $\lambda_{ex} = 525$ nm (1, blank; 2, Ag^+; 3, Cd^{2+}; 4, Co^{2+}; 5, Cr^{3+}; 6, Cu^{2+}; 7, Fe^{3+}; 8, Hg^{2+}; 9, Na^+; 10, Mg^{2+}; 11, Mn^{2+}; 12, Ni^{2+}; 13, Zn^{2+} (100 μM)) Spectra were recorded every 2 min after adding Hg^{2+}.

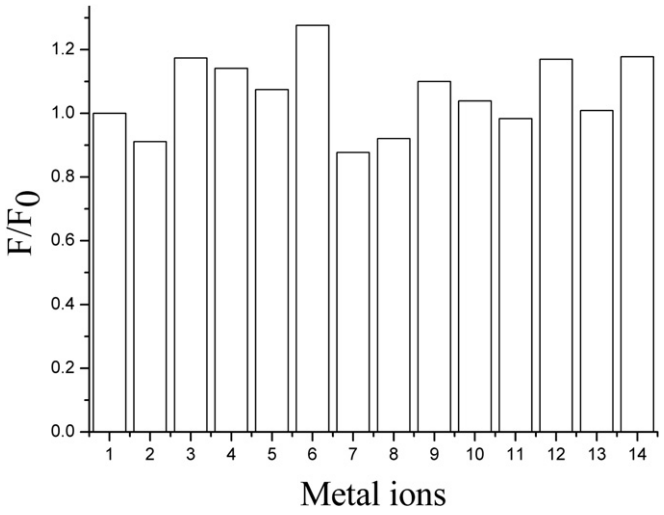

Fig. 6. Fluorescent emission changes of Rho-Fe_3O_4@SiO_2 (0.3 g/L) upon the subsequent addition of 10 equiv of Hg^{2+} to a solution containing 10 equiv of the cation of interest. 1, blank; 2, Ag^{+}; 3, Cd^{2+}; 4, Co^{2+}; 5, Cr^{3+}; 6, Cu^{2+}; 7, Fe^{3+}; 8, Hg^{2+}; 9, Na^{+}; 10, Mg^{2+}; 11, Mn^{2+}; 12, Ni^{2+}; 13, Zn^{2+} (100 μM). Spectra were recorded every 2 min after adding the above cation. ($\lambda_{ex} = 525$ nm).

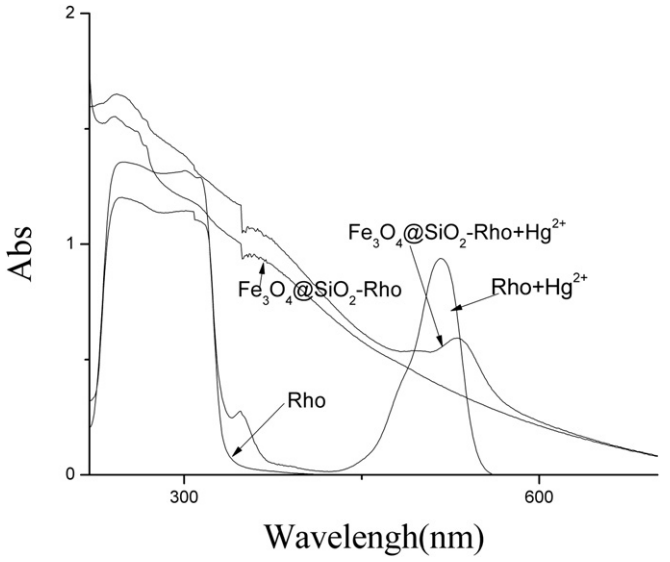

Fig. 8. Absorption spectra of (a) Rho-Si (1×10^{-5} M), (b) Rho-Si + Hg^{2+} (1×10^{-5} M), (c) Rho-Fe_3O_4@SiO_2 (0.3 g/L) and (d) Rho-Fe_3O_4@SiO_2 + Hg^{2+} (0.3 g/L) in CH_3CN solution.

including Ag^{+}, Cd^{2+}, Co^{2+}, Cr^{3+}, Cu^{2+}, Fe^{3+}, Hg^{2+}, Li^{+}, Mg^{2+}, Mn, Ni^{2+} and Zn^{2+} were measured. Fluorescence spectra of a 0.3×10^{-3} kg dm^{-3} solution of Rho-Fe_3O_4@SiO_2 in CH_3CN, corresponding to a concentration of the Rho-Si fluorophore of 2.0×10^{-5} mol dm^{-3}, recorded within 2 min of the addition of 1×10^{-4} mol dm^{-3} of each of these metal ions, are shown in Fig. 4a. When Hg^{2+} was added to the ligand solution, Rho-Fe_3O_4@SiO_2 displays almost 11-fold enhancement in fluorescence intensity at 551 nm. While the introduction of other metal ions, no obvious increase can be observed in the fluorescence spectra except the addition of Cr^{3+} and Fe^{3+} ions gave a small increase in fluorescence intensity. As a comparison, in the presence of other metal ions, Rhoen was not as selective as Rho-Fe_3O_4@SiO_2 for Hg^{2+} detection (Fig. 5b). In addition, the enhancement in fluorescence intensity resulting from the addition of Hg^{2+} ion is not influenced by subsequent addition of other metal ions (Fig. 6). Obviously, a significant change in color from colorless to pink could be observed.

Fig. 7 gives detailed fluorescence changes of Rho-Fe_3O_4@SiO_2 (0.3×10^{-3} kg dm^{-3}) upon gradual titration of Hg^{2+} ion. Upon addition of Hg^{2+} ($0–75 \times 10^{-6}$ mol dm^{-3}), the emission band peaked at about 550 nm attributable to the formation of the ring-opened tautomer of Rho-Fe_3O_4@SiO_2. The nice nonlinear fitting of the fluorescence against metal concentration assuming a 1:1 binding ratio (Hg^{2+}/Rho-Fe_3O_4@SiO_2) suggested a 1:1 binding stoichiometry. The overall binding constant is about 1.64×10^6 [57].

3.6. UV–vis spectrum

Fig. 8 depicts the UV–vis diffuse reflectance spectra of Rho-Si (5×10^{-5} mol dm^{-3}), Rho-Si + Hg^{2+}, Rho-Fe_3O_4@SiO_2 and Rho-Fe_3O_4@SiO_2 + Hg^{2+} (0.3×10^{-3} kg dm^{-3}). ([Hg^{2+}] = 1×10^{-4} mol

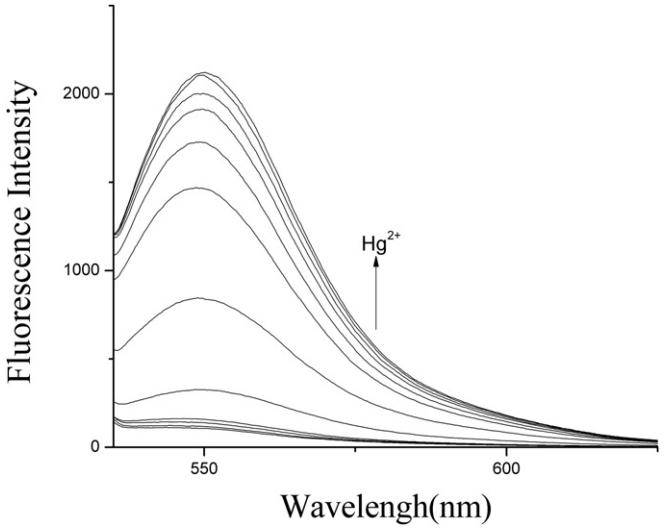

Fig. 7. Fluorescent response of Rho-Fe_3O_4@SiO_2 (0.3 g/L) upon addition of Hg^{2+} (0–75 μM) in CH_3CN, the inset picture shows the fluorescence titration profile around 550 nm at the excitation wavelength of 525 nm. Spectra were recorded every 2 min after adding Hg^{2+}.

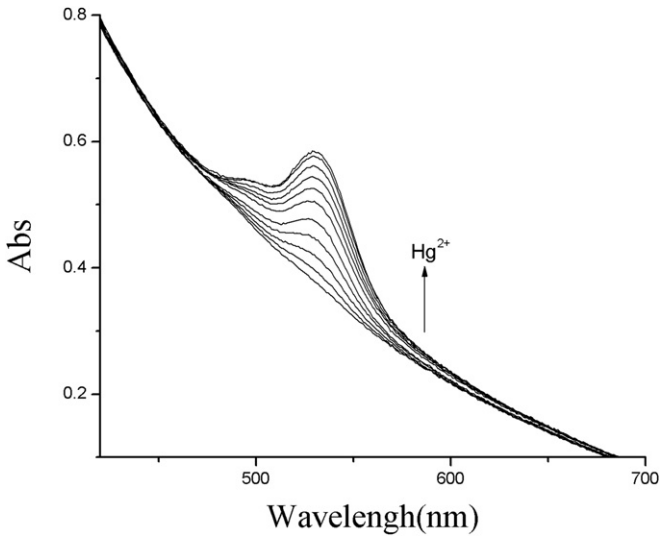

Fig. 9. UV–vis spectra of Rho-Fe_3O_4@SiO_2 (0.3 g/L) in CH_3CN in the presence of different amounts of Hg^{2+} (0–100 μM).

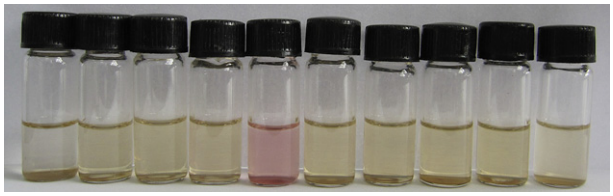

Fig. 10. Color change of Rho-Fe_3O_4@SiO_2 in CH_3CN (0.3 g/L) after addition of 10 equiv of metal ions. Left to right: 1, blank; 2, Ag^+; 3, Cd^{2+}; 4, Cu^{2+}; 5, Hg^{2+}; 6, Fe^{3+}; 7, Co^{2+}; 8, Cr^{3+}; 9, Ni^{2+}; 10, Zn^{2+}. (For interpretation of the references to color in this figure legend, the reader is referred to the web version of this article.)

dm^{-3}) It can be seen that the absorbance peak shifted from 517 nm (Rho-Si + Hg^{2+}) to 529 nm (Rho-Fe_3O_4@SiO_2 + Hg^{2+}). This phenomenon can be further confirmed that Rho-en is successfully conjugated onto the surface of the Fe_3O_4@SiO_2 nanoparticles. Compared with Rho-Si + Hg^{2+}, the fluorescence intensity of Fe_3O_4@SiO_2 + Hg^{2+} is decreased.

The absorption spectra of Rho-Fe_3O_4@SiO_2 with varying Hg^{2+} concentration were recorded, as shown in Fig. 9. Upon the addition of Hg^{2+} to Rho-Fe_3O_4@SiO_2, the peak around 529 nm is significantly enhanced, suggesting the formation of the ring-opened tautomer of Rho-Fe_3O_4@SiO_2 upon Hg^{2+} binding. In this case, the titration solution exhibited an obvious and characteristic color change from colorless to pink. Rho-Fe_3O_4@SiO_2 thus can be used as a "naked-eye" detector of Hg^{2+} (Fig. 10).

4. Conclusion

In summary, we have successfully designed and synthesized magnetic core–shell Fe_3O_4@SiO_2 nanoparticles functionalized by Rho-en which act as a colorimetric and fluorescent chemosensor for Hg(II) in CH_3CN. The selectivity of the Rho-Fe_3O_4@SiO_2 for Hg(II) ion is better than that of the Rho-en. This work provides a platform to prepare magnetic nanoparticles modified by organic fluorescent chemosensor with high affinity, selectivity and sensitivity to detect metal ions.

Acknowledgments

The authors acknowledge the financial support from the NSFC (gs1) (Grant Nos. 20771048, 20931003) and the Fundamental Research Funds for the Central Universities (lzujbky-2009-k06).

References

[1] (a) Zapata F, Caballero A, Espinosa A, Tárraga A, Molina P. Triple channel sensing of Pb(II) ions by a simple multiresponsive ferrocene receptor having a 1-deazapurine backbone. Organic Letters 2008;10:1041–4;
(b) Buie NM, Talanov VS, Butcher RJ, Talanova GG. New fluorogenic dansyl-containing calix[4]arene in the partial cone conformation for highly sensitive and selective recognition of lead(II). Inorganic Chemisry 2008;47:3549–58;
(c) Zapata F, Caballero A, Espinosa A, Tárraga A, Molina P. Imidazole-annelated ferrocene derivatives as highly selective and sensitive multichannel chemical probes for Pb(II) cations. Journal of Organic Chemistry 2009;74:4787–96.

[2] (a) Tang XL, Peng XH, Dou W, Mao J, Zheng JR, Qin WW, et al. Design of a semirigid molecule as a selective fluorescent chemosensor for recognition of Cd(II). Organic Letters 2008;10:3653–6.

[3] (a) Qin H, Ren J, Wang J, Wang E. G-quadruplex facilitated turn-off fluorescent chemosensor for selective detection of cupric ion. Chemical Communication 2010;46:7385–7;
(b) Yin S, Leen V, Van Snick S, Boens N, Dehaen W. A highly sensitive, selective, colorimetric and near-infrared fluorescent turn-on chemosensor for Cu^{2+} based on BODIPY. Chemical Communication 2010;46:6329–31;
(c) Chen J, Zeng F, Wu S, Su J, Zhao J, Tong Z. A facile approach for cupric ion detection in aqueous media using polyethyleneimine/PMMA core–shell fluorescent nanoparticles. Nanotechnology 2009;20:365502.

[4] (a) Kumar M, Dhir A, Bhalla V, Sharma R, Puri RK, Mahajan RK. Highly effective chemosensor for mercury ions based on bispyrenyl derivative. Analyst 2010;135:1600–5;
(b) Zhou Y, Zhu CY, Gao XS, You XY, Yao C. Hg^{2+}-selective ratiometric and "off–on" chemosensor based on the azadiene–pyrene derivative. Organic Letters 2010;12:2566–9;
(c) Zapata F, Caballero A, Espinosa A, Tárraga A, Molina P. A selective redox and chromogenic probe for Hg(II) in aqueous environment based on a ferrocene-azaquinoxaline dyad. Inorganic Chemisry 2009;48:11566–75;
(d) Ho ML, Chen KY, Lee GH, Chen YC, Wang CC, Lee JF, et al. Mercury(II) recognition and fluorescence imaging in vitro through a 3D-complexation structure. Inorganic Chemisry 2009;48:10304–11;
(e) Zou Q, Tian H. Chemodosimeters for mercury(II) and methylmercury(I) based on 2,1,3-benzothiadiazole. Sensors & Actuators: B. Chemical 2010;149:20–7;
(f) Liu B, Tian H. A selective fluorescent ratiometric chemodosimeter for mercury ion. Chemical Communications; 2005:3156–8.

[5] (a) Swamy KMK, Ko SK, Kwon SK, Lee HN, Mao C, Kim JM, et al. Boronic acid-linked fluorescent and colorimetric probes for copper ions. Chemical Communication 2008;45:5915–7;
(b) Joshi BP, Park J, Lee WI, Lee KH. Process sampling module coupled with purge and trap–GC–FID for in situ auto-monitoring of volatile organic compounds in wastewater. Talanta; 2009:903–8.

[6] (a) Boening DW. Ecological effects, transport, and fate of mercury: a general review. Chemosphere 2000;40:1335–51;
(b) Zheng W, Aschner M, Ghersi-Egea JF. Toxicology and Applied Pharmacology 2003;192:1–11;
(c) Mutter J, Naumann J, Schneider R, Walach H, Haley B. Neuroendocrinol Letters 2005;26:439–46.

[7] Fang C, Zhang M. Multifunctional magnetic nanoparticles for medical imaging applications. Journal of Materials Chemistry 2009;19:6258–66.

[8] Gao J, Gu H, Xu B. Multifunctional magnetic nanoparticles: design, synthesis, and biomedical applications. Accounts of Chemical Research 2009;42:1097–107.

[9] Son SJ, Reichel J, He B, Schuchman M, Lee SB. Magnetic nanotubes for magnetic-field-assisted bioseparation, biointeraction, and drug delivery. Journal of the American Chemical Society 2005;127:7316–7.

[10] Abou-Hassan A, Bazzi R, Cabuil V. Multistep continuous-flow microsynthesis of magnetic and fluorescent-Fe_2O_3@SiO_2 core/shell nanoparticles. Angewandte Chemie, International Edition 2009;48:7180–3.

[11] Insin N, Tracy JB, Lee H, Zimmer JP, Westervelt RM, Bawendi MG. Incorporation of iron oxide nanoparticles and quantum Dots into silica microspheres. ACS Nano; 2008:2197–202.

[12] Zhu YH, Da H, Yang X, Hu Y. Preparation and characterization of core–shell monodispersed magnetic silica microspheres. Colloids and Surfaces A: Physicochemical and Engineering Aspects 2003;231:123–9.

[13] (a) See KH, Mullins ME, Mills OP, Heiden PA. A reactive core–shell nanoparticle approach to prepare hybrid nanocomposites: effects of processing variables. Nanotechnology 2005;16:1950–9;
(b) Baby TT, Ramaprabhu S. SiO_2 coated Fe_3O_4 magnetic nanoparticle dispersed multiwalled carbon nanotubes based amperometric glucose biosensor. Talanta 2010;80:2016–22.

[14] (a) Liu ZM, Liu YL, Yang HF, Yang Y, Shen GL, Yu RQ. A phenol biosensor based on immobilizing tyrosinase to modified core–shell magnetic nanoparticles supported at a carbon paste electrode. Analytica Chimica Acta 2005;533:3–9;
(b) Schätz A, Hager M, Reiser O. Cu(II)–Azabis(oxazoline)-complexes immobilized on superparamagnetic magnetite@silica-nanoparticles: a highly selective and recyclable catalyst for the kinetic resolution of 1,2-diols. Advanced Functional Materials 2009;19:2109–15.

[15] (a) Lesnikovich AI, Shunkevich TM, Naumenko VN, Vorobyova SA, Baykov MV. Dispersity of magnetite in magnetic liquids and the interaction with a surfactant. Journal of Magnetism and Magnetic Materials 1990;85:14–6;
(b) Laurent S, Forge D, Port M, Roch A, Robic C, Elst LV, et al. Magnetic iron oxide nanoparticles: synthesis, stabilization, vectorization, physicochemical characterizations, and biological applications. Chemical Reviews 2008;108:2064–110.

[16] Sun Y, Duan L, Guo Z, Duan Y, Ma M, Xu L, et al. An improved way to prepare superparamagnetic magnetite–silica core–shell nanoparticles for possible biological application. Journal of Magnetism and Magnetic Materials 2005;285:65–70.

[17] Dujols V, Ford F, Czarnik AW. A long-wavelength fluorescent chemodosimeter selective for Cu(II) ion in water. Journal of the American Chemical Society 1997;119:7386–7.

[18] Xiang Y, Mei L, Li N, Tong AJ. Sensitive and selective spectrofluorimetric determination of chromium(VI) in water by fluorescence enhancement. Analytica Chimica Acta 2007;581:132–6.

[19] Weerasinghe AJ, Schmiesing C, Sinn E. Highly sensitive and selective reversible sensor for the detection of Cr^{3+}. Tetrahedron Letters 2009;50:6407–10.

[20] Huang K, Yang H, Zhou Z, Yu M, Li F, Gao X, et al. Multisignal chemosensor for Cr^{3+} and its application in bioimaging. Organic Letters 2008;10:2557–60.

[21] Moon KS, Yang YK, Ji S, Tae J. Aminoxy-linked rhodamine hydroxamate as fluorescent chemosensor for Fe^{3+} in aqueous media. Tetrahedron Letters 2010;51:3290–3.

[22] Bae S, Tae J. Rhodamine-hydroxamate-based fluorescent chemosensor for Fe^{III}. Tetrahedron Letters 2007;48:5389–92.

[23] Zhang X, Shiraishi Y, Hairi T. Fe(III)- and Hg(II)-selective dual channel fluorescence of a rhodamine–azacrown ether conjugate. Tetrahedron Letters 2008;49:4178–81.
[24] Zhang M, Gao Y, Li M, Yu M, Li F, Li L, et al. A selective turn-on fluorescent sensor for Fe^{III} and application to bioimaging. Tetrahedron Letters 2007;48:3709–12.
[25] Zhang X, Shiraishi Y, Hirai T. A new rhodamine-based fluorescent chemosensor for transition metal cations synthesized by one-step facile condensation. Tetrahedron Letters 2007;48:5455–9.
[26] Xiang Y, Tong AJ, Jin PY, Ju Y. New fluorescent rhodamine hydrazone chemosensor for Cu(II) with high selectivity and sensitivity. Organic Letters 2006;8:2863–6.
[27] Chen X, Jou MJ, Lee H, Kou S, Lim J, Nam SW, et al. New fluorescent and colorimetric chemosensors bearing rhodamine and binaphthyl groups for the detection of Cu^{2+}. Sensors and Actuators B: Chemical 2009;137:597–602.
[28] Zhou Y, Wang F, Kim Y, Kim SJ, Yoon J. Cu^{2+}-selective ratiometric and "off–on" sensor based on the rhodamine derivative bearing pyrene group. Organic Letters 2009;11:4442–5.
[29] Zhang X, Shiraishi Y, Hirai T. Cu(II)-selective green fluorescence of a rhodamine-diacetic acid conjugate. Organic Letters 2007;9:5039–42.
[30] Lee MH, Kim HJ, Yoon S, Park N, Kim JS. Metal ion induced FRET OFF–ON in tren/dansyl-appended rhodamine. Organic Letters 2008;10:213–6.
[31] Zheng H, Qian ZH, Xu L, Yuan FF, Lan LD, Xu JG. Switching the recognition preference of rhodamine B spirolactam by replacing one atom: design of rhodamine B thiohydrazide for recognition of Hg(II) in aqueous solution. Organic Letters 2006;8:859–61.
[32] Lee MH, Wu JS, Lee JW, Jung JH, Kim JS. Highly sensitive and selective chemosensor for Hg^{2+} based on the rhodamine fluorophore. Organic Letters 2007;9:2501–4.
[33] Wu D, Huang W, Duan C, Lin Z, Meng Q. Highly sensitive fluorescent probe for selective detection of Hg^{2+} in DMF aqueous media. Inorganic Chemistry 2007;46:1538–40.
[34] Yang YK, Yook KJ, Tae J. A rhodamine-based fluorescent and colorimetric chemodosimeter for the rapid detection of Hg^{2+} ions in aqueous media. Journal of the American Chemical Society 2005;127:16760–1.
[35] Ko SK, Yang YK, Tae J, Shin I. In vivo monitoring of mercury ions using a rhodamine-based molecular probe. Journal of the American Chemical Society 2006;128:14150–5.
[36] Wu JS, Hwang IC, Kim KS, Kim JS. Rhodamine-based Hg^{2+}-selective chemodosimeter in aqueous solution: fluorescent OFF–ON. Organic Letters 2007;9:907–10.
[37] Shi W, Ma H. Rhodamine B thiolactone: a simple chemosensor for Hg^{2+} in aqueous media. Chemical Communication; 2008:1856–8.
[38] Zhang X, Xiao Y, Qian X. A ratiometric fluorescent probe based on FRET for imaging Hg^{2+} ions in living cells. Angewandte Chemie International Edition 2008;47:8025–9.
[39] Wu D, Huang W, Lin Z, Duan Ch, He C, Wu S, et al. Highly sensitive multi-responsive chemosensor for selective detection of Hg^{2+} in natural water and different monitoring environments. Inorganic Chemisry 2008;47:7190–201.
[40] Zhan XQ, Qian ZH, Zheng H, Su BY, Lan Z, Xu JG. Rhodamine thiospirolactone. Highly selective and sensitive reversible sensing of Hg(II). Chemical Communication; 2008:1859–61.
[41] Soh JH, Swamy KMK, Kim SK, Kim S, Lee SH, Yoon J. Rhodamine urea derivatives as fluorescent chemosensors for Hg^{2+}. Tetrahedron Letters 2007;48:5966–9.
[42] Yang H, Zhou ZG, Huang KW, Yu MX, Li FY, Yi T, et al. Multisignaling optical electrochemical sensor for Hg^{2+} based on a rhodamine derivative with a ferrocene unit. Organic Letters 2007;9:4729–32.
[43] Suresh M, Shrivastav A, Mishra S, Suresh E, Das A. A rhodamine-based chemosensor that works in the biological system. Organic Letters 2008;10:3013–6.
[44] Huang W, Song C, He C, Lv G, Hu X, Zhu X, et al. Recognition preference of rhodamine-thiospirolactams for mercury(II) in aqueous solution. Inorganic Chemistry 2009;48:5061–72.
[45] Kwon JY, Jang YJ, Lee YJ, Kim KM, Seo MS, Nam W, et al. A highly selective fluorescent chemosensor for Pb^{2+}. Journal of the American Chemical Society 2005;127:10107–11.
[46] Peng X, Du J, Fan J, Wang J, Wu Y, Zhao J, et al. A selective fluorescent sensor for imaging Cd^{2+} in living cells. Journal of the American Chemical Society 2007;129:1500–1.
[47] Chatterjee A, Santra M, Won N, Kim S, Kim JK, Kim SB, et al. Selective fluorogenic and chromogenic probe for detection of silver ions and silver nanoparticles in aqueous media. Journal of the American Chemical Society 2009;131:2040–1.
[48] Shi W, Sun S, Li X, Ma H. Imaging different interactions of mercury and silver with live cells by a designed fluorescence probe rhodamine B selenolactone. Inorganic Chemistry 2010;49:1206–10.
[49] Kim YR, Kim HJ, Kim JS, Kim H. Rhodamine-Based "Turn-On" fluorescent chemodosimeter for Cu(II) on ultrathin platinum films as molecular switches. Advanced Materials 2008;20:4428–32.
[50] Ma BL, Wu SZ, Zeng F, Luo YL, Zhao JQ, Tong Z. Nanosized diblock copolymer micelles as a scaffold for constructing a ratiometric fluorescent sensor for metal ion detection in aqueous media. Nanotechnology 2010;21:195501.
[51] (a) Meng QT, Zhang XL, He C, He GJ, Zhou P, Duan CY. Multifunctional mesoporous silica material used for detection and adsorption of Cu^{2+} in aqueous solution and biological applications in vitro and in vivo. Advanced Functional Materials 2010;20:1903–9;
(b) Zhou P, Meng QT, He GJ, Wu HM, Duan CY, Quan X. Highly sensitive fluorescence probe based on functional SBA-15 for selective detection of Hg^{2+} in aqueous media. Journal of Environmental Monitoring 2009;11:648–53;
(c) Leng B, Jiang JB, Tian H. A mesoporous silica supported Hg^{2+} chemodosimeter. American Institute of Chemical Engineers 2010;56:2957–64.
[52] (a) Wang BD, Hai J, Liu ZC, Wang Q, Yang ZY, Sun SH. Selective detection of Iron(III) by rhodamine-modified Fe_3O_4 nanoparticles. Angewandte Chemie, International Edition 2010;49:1–5;
(b) Leng B, Zou L, Jiang JB, Tian H. Colorimetric detection of mercuric ion (Hg^{2+}) in aqueous media using chemodosimeter-functionalized gold nanoparticles. Sensors and Actuators B: Chemical 2009;140:162–9.
[53] Molday RS. Magnetic iron–dextran microspheres. U.S. Patent 4. 1984; 452:773.
[54] Lu CW, Lu CW, Hung Y, Hsiao JK, Yao M, Chung TH, et al. Bifunctional magnetic silica nanoparticles for highly efficient human stem cell labeling. Nano Letters 2007;7:149–54.
[55] (a) Wang X, Wang LY, He XW, Zhang YK, Chen LX. A molecularly imprinted polymer-coated nanocomposite of magnetic nanoparticles for estrone recognition. Talanta 2009;78:327–32;
(b) Wang JH, Zheng SR, Shao Y, Liu JL, Xu ZY, Zhu DQ. Amino-functionalized Fe_3O_4@SiO_2 core–shell magnetic nanomaterial as a novel adsorbent for aqueous heavy metals removal. Journal of Colloid and Interface Science 2010;349:293–9.
[56] Lin YS, Haynes CL. Synthesis and characterization of biocompatible and size-tunable multifunctional porous silica nanoparticles. Chemistry Materials 2009;21:3979–86.
[57] Connors KA. Binding constants complex stability. New York: John Wiley & Sons; 1987. pp. 24–28.